Effects of Sulfate on Biotite Interfacial Reactions under High Temperature and High CO_2 Pressure

Journal:	*Physical Chemistry Chemical Physics*
Manuscript ID	CP-ART-11-2018-007368.R1
Article Type:	Paper
Date Submitted by the Author:	13-Feb-2019
Complete List of Authors:	Zhang, Lijie; Washington University in Saint Louis, Energy, Environmental and Chemical Engineering Zhu, Yaguang; Washington University in Saint Louis, Energy, Environmental and Chemical Engineering Wu, Xuanhao; Washington University in Saint Louis, Energy, Environmental & Chemical Engineering Jun, Young-Shin; Washington University, Energy, Environment and Chemical Engnieering

Effects of Sulfate on Biotite Interfacial Reactions under High Temperature and High CO_2 Pressure

Lijie Zhang, Yaguang Zhu, Xuanhao Wu, and Young-Shin Jun*

Department of Energy, Environmental and Chemical Engineering,

Washington University in St. Louis, St. Louis, MO 63130

Address: One Brookings Drive, Campus Box 1180

E-mail: ysjun@seas.wustl.edu

Phone: (314)935-4539

Fax: (314)935-7211

http://encl.engineering.wustl.edu/

Submitted: February 2019

Physical Chemistry Chemical Physics

*Corresponding Author

ABSTRACT

To ensure the safety and efficiency of engineered subsurface operations, it is vital to understand impacts of aqueous chemistries on brine−mineral interactions in subsurface environments. In this study, using biotite as a model phyllosilicate, we investigated the effects of sulfate on its interfacial reactions under subsurface relevant conditions (95 °C and 102 atm of CO_2). By making monodentate mononuclear complexes with biotite surface sites, 50 mM sulfate enhanced biotite dissolution by 40% compared to that without sulfate. However, sulfate at lower concentrations than 50 mM did not obviously affect biotite dissolution. In addition, sulfate did not impact secondary mineral precipitation. However, even without any discernible surface morphological change, sulfate adsorption made biotite surfaces more hydrophilic. To provide a more comprehensive perspective on environmentally-abundant ligands, we further comparatively examined the effects of various inorganic (e.g., sulfate and phosphate) and organic ligands (e.g., acetate, oxalate, and phosphonates) on biotite interfacial interactions and assessed their impacts on physico-chemical properties. We found that the presence of phosphate and phosphonates significantly promoted precipitation of Fe- and Al-bearing secondary minerals, but sulfate, acetate, and oxalate did not. Biotite surface wettability was also altered as a result of changes in biotite surface functional groups and surface charges by ligand adsorption: sulfate, oxalate, phosphate, and phosphonate made biotite more hydrophilic, while acetate made it more hydrophobic. This study provides useful, new insights into the effects of brine chemistries on brine–mineral interactions, enabling more efficient and safer engineered subsurface operations.

1. Introduction

Subsurface energy sources satisfy over 80% of total U.S. energy needs,[1] and the subsurface also provides ample reservoirs for CO_2 storage, environmental management, waste disposal, and energy storage.[1] Hence, engineered subsurface operations have recently received increasing attention to meet energy demands, mitigate global warming, and manage wastes. The field sites for these operations are usually deeper than 800 m, where the temperature and pressure can range from 31 °C to 110 °C and from 73.8 atm to 600 atm, respectively.[2-4] Because geophysical properties of the reservoirs, such as their wettability, porosity, and permeability, affect the fate, transport, and distribution of related fluids, they are important factors determining the safety and efficiency of subsurface operations. Recent studies found that geochemical processes, such as mineral dissolution and secondary mineral precipitation, can change the geophysical properties of reservoirs.[5-10] Therefore, we need a deeper understanding of geochemical processes of reservoir minerals under subsurface conditions.

Shales are abundant in reservoirs and play key roles in subsurface engineered processes because of their low permeability for trapping and sealing.[11-15] Clay minerals (phyllosilicates) are main constituents of shales, with a minimum mass fraction of about 40%.[16-19] Phyllosilicates have layered structures, containing framework cations occupying tetrahedral and octahedral sheets, and interlayer cations to balance charge.[20-21] During their dissolution, the release of interlayer cations is mainly through ion-exchange reactions with aqueous protons or cations,[22] and the release of framework cations is through proton-mediated or ligand-mediated reactions.[23] Moreover, the dissolution of minerals and consequential release of metal ions will change saturation conditions of the solutions, leading

to secondary mineral precipitation. Thus, the dissolution of phyllosilicates strongly depends on the aqueous chemistry conditions, and further affects subsequent secondary mineral precipitation.

Among many aqueous ions in formation brine, sulfate (SO_4^{2-}) concentrations range from 0.01 M to 0.05 M.[24-27] For example, the sulfate concentration is around 0.03 M in the Weyburn CO_2-injection enhanced oil recovery site and is around 0.04 M in the Ketzin CO_2 storage site.[26-27] Moreover, through numerical simulations, Xu et al. predicted that sulfate concentrations become even higher (~0.8 M) during co-injection of CO_2 and H_2S or SO_2.[28] Under high temperature and high CO_2 pressure conditions, previous studies have reported promotion effects by sulfate on anorthite dissolution[29] and less wellbore cement deterioration with sulfate.[30] However, the effects of sulfate on phyllosilicate dissolution have not been fully investigated yet. In addition, regarding the wettability alteration effects of sulfate, it has been reported that the introduction of seawater containing SO_4^{2-} ions can modify oil-wet calcite to a more water-wet state, thus reducing the capillary pressure barrier and improving the oil recovery efficiency in carbonate formations.[31-35] It has also been reported that as temperature increased, sulfate increased the wettability of chalk, and, thus, the efficiency of enhanced oil recovery.[33] However, we still have limited information about the influence of sulfate on the wettability of phyllosilicates, which are the main components of the shales typical of unconventional oil/gas recovery sites, especially under relevant subsurface conditions.

Along with sulfate, phosphate (0–0.02 mM), acetate (16–250 mM), and oxalate (0–5 mM) are also naturally found in formation brines.[25, 36-37] Moreover, because supercritical CO_2 ($scCO_2$) is a good organic solvent, the concentrations of some organic compounds in brines

(mainly formate and acetate) can increase after $scCO_2$ injection, as reported in a recent study on the Frio formation[37]. In addition to these naturally existing aqueous species, chemical additives are injected into subsurface sites during engineered operations, such as geologic CO_2 storage, conventional/unconventional enhanced oil/gas recovery (EOR), and geothermal applications.[38-39] Among the chemical additives, phosphonate-based scale inhibitors, with an average concentration of ~0.5 mM, are utilized to inhibit the formation of scale minerals that can reduce the porosity and permeability of wellbores and the cracked reservoir rocks, or can block flow in production wells.[40-44] Further, degradation of these phosphonate-based scale inhibitors can release phosphate and increase phosphate concentrations in brines to around 1–2 mM,[45-49] impacting the performance of scale inhibitors. As described above, the diverse brine chemistries significantly affect the dissolution/precipitation of minerals and their subsequent responses to fluid interactions (e.g., wettability), affecting fluid transport. It will be critically useful to have a systematic comparison of the effects of different ligands on brine–mineral interactions under conditions relevant to subsurface environments.

Hence, the goal of this study was to provide insights into the effects of sulfate on brine−phyllosilicate interactions and the subsequent wettability alterations under conditions relevant to subsurface environments. Biotite was used as a model phyllosilicate mineral, and the sulfate concentrations were chosen to be relevant field site conditions.[24-27] Moreover, based on our previously published work, we systematically analyzed and compared the effects of sulfate with other environmentally-abundant inorganic and organic ligands in brine. Then, we discussed the underlying mechanisms of their effects on mineral dissolution, secondary precipitation, and alterations of mineral surface morphology and wettability. For this comparison, to broadly apply our findings to the diverse properties of brines in multiple

field sites, we focused on investigating individual anion/ligand effects (not mixtures of them) on brine−phyllosilicate interactions. Our findings will benefit future studies on the effects of multiple ions/ligands on brine−phyllosilicate interactions. Ultimately, the information presented in this study can help us better assess the roles of a wide spectrum of ligands in brines in the geochemical processes of minerals, and predict their subsequent impacts on the wettability, porosity, and permeability of subsurface reservoirs.

2. Experimental

2.1 Chemicals and Minerals

All chemicals used were American Chemical Society (ACS) grade or higher. To simulate subsurface brine conditions, sulfate solutions with different concentrations, 0 (control), 1 mM, 10 mM, and 50 mM, were prepared in 1.0 M NaCl with deionized (DI) water (resistivity > 18.2 MΩ·cm, Barnstead Ultrapure Water Systems). Detailed chemical information about all the ligands can be found in Table S1 in the ESI.

The biotite used in this study originated from Bancroft, Ontario, Canada, and was purchased from Ward's Natural Science. The chemical composition of the biotite was $K_{0.91}Na_{0.08}Ca_{0.005}(Mg_{0.57}Mn_{0.02}Fe_{0.37}Ti_{0.04})_3(Al_{1.00}Si_{3.00})O_{10}(F_{0.51}(OH)_{0.49})_2$, as analyzed by X-ray fluorescence (XRF).[50] Biotite flakes freshly cleaved along the {001} basal planes were cut into 2.0 cm × 0.8 cm rectangles with a thickness of 80 ± 10 μm (measured with a Vernier caliper). The biotite flakes were sonicated successively in acetone, ethanol, and isopropanol for 5 mins each to remove organic contaminants, then rinsed with DI water and dried with high purity nitrogen gas. The prepared biotite flakes were stored in dust-free tubes for further dissolution experiments.

2.2 High Temperature and High Pressure Reactions

Laboratory biotite dissolution experiments were conducted in a 300 mL high-temperature and high-pressure reactor (Parr Instrument Co., IL), as used in our previous studies (Figure S1, ESI).[50-53] To mimic field site pressure (73.8–600 atm) and temperature (31–110 °C) conditions and to obtain results comparable with previous reports,[2-4, 50-55] the experimental pressure was 102 atm CO_2 and the temperature was 95 °C. The initial pH of the control solution (without sulfate) at the experimental pressure and temperature conditions was around 3.2, calculated by Geochemist's Workbench (GWB, Release 8.0). Detailed information about the thermodynamic calculations can be found in S2 in the ESI. Hence, the pH of the sulfate solutions was adjusted to give the systems the same initial pH as the control system at 95 °C and 102 atm CO_2. Due to the high salinity (1.0 M NaCl) in the solutions, the additions of hydrochloric acid (HCl) and sodium hydroxide (NaOH) during pH adjustment did not much affect the ionic strength. Duplicate biotite flakes were reacted in the prepared solutions for desired time intervals (3, 8, 22, 70, and 96 h). Triplicate experiments were conducted. The experiments provided information on brine−biotite interactions in the early period of $scCO_2$-enhanced engineered subsurface operations.

After the reactions, the reactor was slowly degassed by releasing the pressure valve and allowed to cool. The degassing process took about 0.5 h, which was controlled to be the same for different reaction conditions. According to our previous studies, the decrease of temperature and degassing of CO_2 should not affect the surface properties/secondary precipitate formation.[50, 56] The obtained solution samples were filtered through 0.2 μm polypropylene membranes and acidified in 1% trace metal nitric acid (HNO_3). The aqueous solutions were then analyzed with inductively coupled plasma-optical emission spectrometry

(ICP-OES, PerkinElmer Optima 7300 DV) to determine their dissolved ion concentrations, and measured with ion chromatography (IC, Thermo Scientific Dionex ICS-1600) to get the residual sulfate concentrations in the solutions. The sulfate adsorption in each system was calculated as the difference between the initial and residual sulfate concentrations (from IC results) normalized by the initial biotite geometric surface areas. The pH values after 96 h reaction were calculated by taking ICP-OES and IC results as input for GWB calculations (S2, ESI).

2.3 Characterization of the Surface Morphology of Reacted Biotite

The reacted biotite flakes were rinsed with DI water to remove extra ions from brine, dried with high purity nitrogen, and then used for further characterizations. For surface morphology, the rinsed reacted biotite flakes were mounted onto steel pucks for imaging with atomic force microscopy (AFM, Nanoscope V Multimode SPS, Veeco). AFM measurements were conducted under ambient conditions in contact mode. Using nonconductive silicon nitride probes (tip radius of 10 nm, DNP-S10, Bruker), the biotite's basal surface was scanned at a rate of 0.999 Hz and a deflection setpoint of 1.975 V. The collected AFM images were analyzed with Nanoscope software (v7.20). Statistical information about height, crack depth, and root-mean-square surface roughness (R_q) was obtained through the analyses and is shown in S3 in the ESI.

2.4 Measurement of Water Contact Angles

Wettability alteration is indicated by changes in water contact angles. Under ambient conditions, using a contact analyzer (Surface Electro Optics, Phoenix 300), contact angles were measured for biotite samples reacted without and with sulfate in the high temperature

and high pressure systems. Additionally, biotite samples reacted with 10 mM acetate and 10 mM oxalate, as described in a previous study,[50] were also characterized for contact angles. Droplets of DI water, minimizing potential effects of ionic strength on contact angle measurements, were placed on reacted biotite basal surfaces, and images were taken with a high-resolution camera (Zoom 7000, Navitar). At least six measurements were made on every biotite sample. Contact angles were then obtained by analyzing the images (Surfaceware 8.0).[52] Note that the absolute values of contact angles measured under ambient conditions can be different from those measured at high temperature and CO_2 pressure. However, in our previous report, we found that the contact angle results obtained under ambient conditions followed the same trend in contact angles biotite samples reacted in different systems (high CO_2 pressure and high temperature).[52]

2.5 Analysis of Sulfate Complexation by Fourier Transformation Infrared (FTIR) Spectroscopy

To investigate the types of sulfate−biotite surface complexes, attenuated total reflectance (ATR)-FTIR spectra were collected using a Thermo Scientific Nicolet iS10 spectrometer with a horizontal Ge ATR crystal. Using a method described in our previous study,[52] briefly, clean biotite flakes were ground with stainless steel blades, and particles in the size range of 53–106 μm were collected. The biotite particles were then sonicated in ethanol to detach tiny particles, and the suspension was allowed to settle for 3 hours. The supernatant was collected, and the size of the particles was measured by dynamic light scattering as around 100 nm. Then the biotite particles were deposited onto the Ge crystal, and allowed to dry. Solutions were prepared of (a) 1 M NaCl, (b) 1 M NaCl + 1 mM sulfate,

(c) 1 M NaCl + 10 mM sulfate, and (d) 1 M NaCl + 50 mM sulfate. All three solutions had an initial pH of 3.16, which was the initial pH of the same reaction solutions under 95 °C and 102 atm of CO_2. Next, 1 mL of the prepared solution was added to the crystal and allowed to contact the dried biotite particle film. Four hundred scans were collected with a resolution of 1 cm^{-1}. Then, the spectrum of biotite contacting solution (a) was used as a background and subtracted from the spectra of biotite contacting solutions (b), (c), and (d).

3. Results and Discussion

3.1 Effects of Sulfate on Biotite Dissolution

The effects of sulfate on the evolutions of aqueous cation concentrations in the reaction systems are shown in Figure 1. Regarding interlayer K^+, similar aqueous concentrations were observed in all the four reaction solutions. It is known that the release of interlayer cations (K^+ in the case of biotite) is through ion-exchange reactions with cations in the solution.[22] The ionic strength and initial pH were controlled to be the same for the different reaction solutions, and there were no significant differences in the final pH values of the solutions after reaction with biotite for 96 h. As calculated by GWB, the pH values were 3.4±0.1 for the control, 3.4±0.1 for 1 mM sulfate, 3.5±0.1 for 10 mM sulfate, and 3.4±0.1 for 50 mM sulfate. Therefore, the concentration levels of H^+ and Na^+ in all the reaction systems should be close, resulting in similar extents of ion-exchange reactions between interlayer K^+ and cations in the solutions.

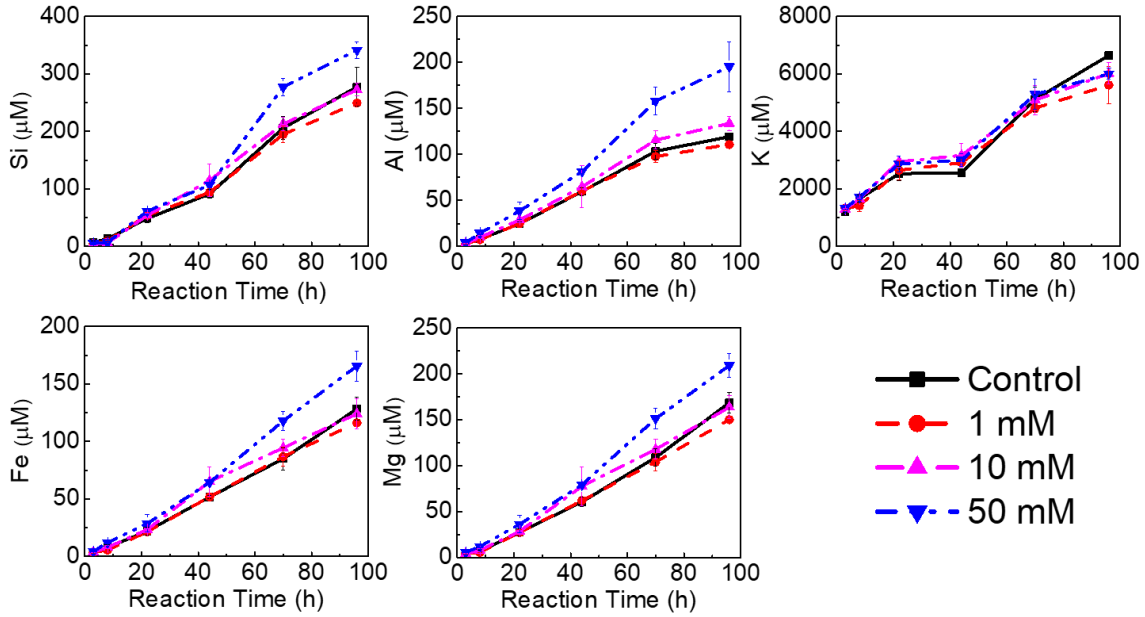

Figure 1 Aqueous concentrations of Si, Al, Fe, Mg, and K from dissolution of biotite at 95 °C and 102 atm CO_2, with an ionic strength of around 1.0 M and an initial pH of 3.16, in 0, 1, 10, and 50 mM sulfate solutions. Error bars are the standard deviations of duplicate samples in triplicate experiments.

However, the concentration evolutions of framework cations, i.e., Si, Mg, Fe, and Al, differed in response to concentrations of sulfate. The effects of low sulfate concentrations (1 mM and 10 mM) were not discernable from that in the control experiment, while the presence of 50 mM sulfate promoted the release of framework cations by about 40%. Because the pH values of the reaction systems were close, the proton-mediated dissolution reaction cannot be the responsible dissolution pathway. Interestingly, in a recent study, Min et al. reported that the dissolution of anorthite ($CaAl_2Si_2O_8$) was enhanced by 50 mM sulfate by 36%,[29] a value very close to our finding in this study. In their system, aqueous complexation was not the main mechanism for the enhancement. In our experimental system, according to

thermodynamic calculations using GWB, the main aqueous species of sulfate was SO_4^{2-}, and its aqueous complexation with metal ions (e.g., Fe^{2+}/Fe^{3+}, Al^{3+}, Na^+, and K^+) was very weak due to low stability constants (less than 10^3).[57] Hence, aqueous complexation was also not the mechanism for the promotion effects of 50 mM sulfate on biotite dissolution. Min et al. further explained that the formation of inner-sphere monodentate complexes between sulfate and the tetrahedral aluminum sites on anorthite surfaces was responsible for the enhancement effects of sulfate on anorthite dissolution. Thus, we hypothesized that the formation of surface complexes between sulfate and biotite tetrahedral aluminum sites could also occur to promote biotite dissolution in our reaction systems.

3.2 Sulfate Complexation and Adsorption on Biotite Surfaces

To test the hypothesis that sulfate forms surface complexes with biotite, ATR-FTIR spectra of sulfate contacted with biotite were measured and are shown in Figure 2. Although aqueous sulfate has an asymmetric stretching at 1100 cm^{-1}, we observe that the band centered at 1100 cm^{-1} is broad between 1050 cm^{-1} and 1140 cm^{-1}. Serna et al. reported that this feature corresponds to monodentate mononuclear surface complexes between sulfate and Al oxide,[58] which also occurred in our reaction systems. The sulfate adsorption geometry on biotite would likely have a corner shared oxygen between sulfate and Al-substituted tetrahedron, as suggested in a previous study.[29] In addition, because the basal surface of biotite has a negative charge and the oxygen in the basal surface is fully saturated, sulfate adsorption will not occur easily on the basal surface. Therefore, it is most likely that sulfate adsorption occurs on the edges of biotite, where broken bonds result in the formation of unsaturated surface oxygen that can enable (de)protonation and (ligand) exchange. Then, monodentate mononuclear

surface complexes can promote mineral dissolution by polarizing metal-oxygen bonds and can facilitate the detachment of surface metal species.[59] Furthermore, we also observed similar intensities of monodentate mononuclear surface complexes in the presence of 1 mM and 10 mM sulfate, but a higher intensity was observed with 50 mM sulfate, indicating a more significant extent of surface complexation. Correspondingly, after 8 h high temperature and high pressure reaction, a larger amount of sulfate adsorption was observed as the initial sulfate concentrations increased (inset in Figure 2). The amounts of sulfate adsorption in the 10 mM and 50 mM system were not significantly different, indicating that the biotite surface was almost saturated with sulfate. While the surface complexation with 1 mM and 10 mM sulfate was not sufficient to induce observable promotion effects on biotite dissolution, the enhancement effects were most obvious with 50 mM sulfate, as observed in Figure 1. Here, binuclear surface complexes are not expected on biotite, owing to the Al avoidance principle,[29, 60] namely, there are no available Al sites adjacent to each other in biotite to form binuclear surface complexes. The peak at around 1025 cm^{-1} was attributed to the Si–O band of biotite,[61] which was not fully subtracted, even after the background correction. The sulfate adsorption in the 1 mM system was very low, so the 1 mM sulfate system might be more sensitive to background subtraction, causing its absorbance spectrum to be closely similar to that of the 10 mM sulfate system.

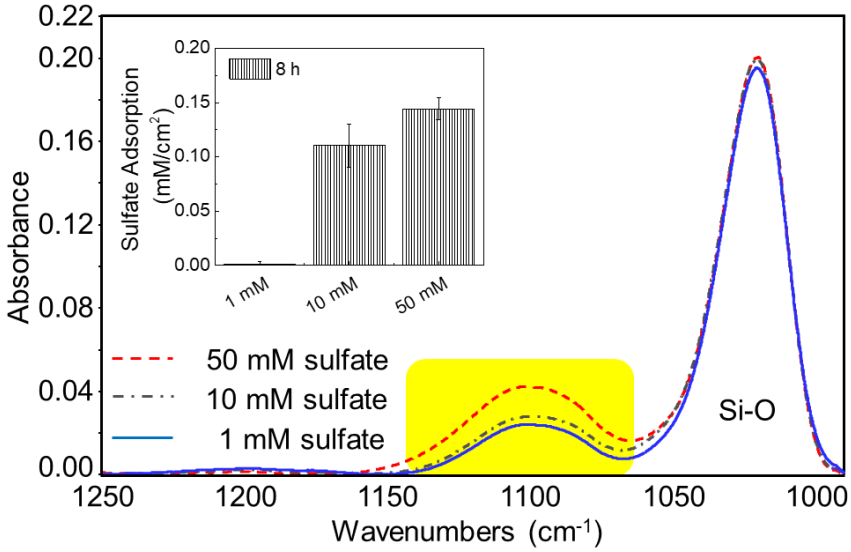

Figure 2 ATR-FTIR spectra of biotite contacted with different concentrations of sulfate. The spectrum of biotite contacted with 1 M NaCl was used as background. Inset: Amount of sulfate adsorbed onto biotite after 8 h reaction with different initial concentrations of sulfate under 95 °C and 102 atm CO_2.

3.3 Effects of Sulfate on Biotite Surface Morphology and Wettability

Based on AFM imaging, the presence of different concentrations of sulfate did not significantly affect the morphological evolutions of reacted biotite basal surfaces, shown in Figure S2 and Figure 3. Fibrous precipitates, identified to be fibrous illite formed by oriented aggregation of small hexagonal nanoparticles on samples after reaction in 1 M NaCl in a previous study,[62] were also observed on biotite basal surfaces after 3 h reaction with sulfate (Figure S2). In addition, after reactions of 22 h and longer, cracks were formed on reacted biotite basal surfaces, as a result of ion-exchange reactions of aqueous Na^+ with biotite interlayer K^+, dissolution of framework cations, and CO_2 intercalation.[50, 62] The cracks

exposed new edge surface sites on the reacted biotite basal surfaces, where sulfate could also form complexes.

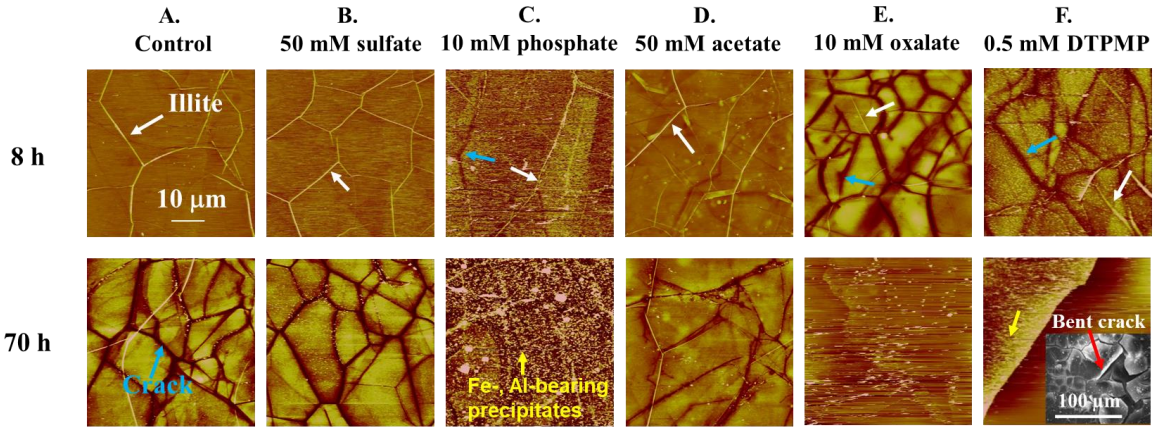

Figure 3 Height mode AFM observations of biotite basal surfaces after reaction at 95 °C and 102 atm CO_2 with different brine chemistries. The AFM images are 50 μm × 50 μm. The height scale is 60 nm for images A, B, C, D, E-8 h, and F-8 h, is 100 nm for E-72 h, and is 200 nm for F-70 h. The different height scales show the results more clearly. Inset in F-70 h is an SEM image of the corresponding sample. The arrows in the same colors point to similar surface features. The images of C, D, E, and F are reproduced from refs. 47, 49, 50, and 52. Copyright 2015 and 2018 American Chemical Society and Copyright 2017 Royal Society of Chemistry.

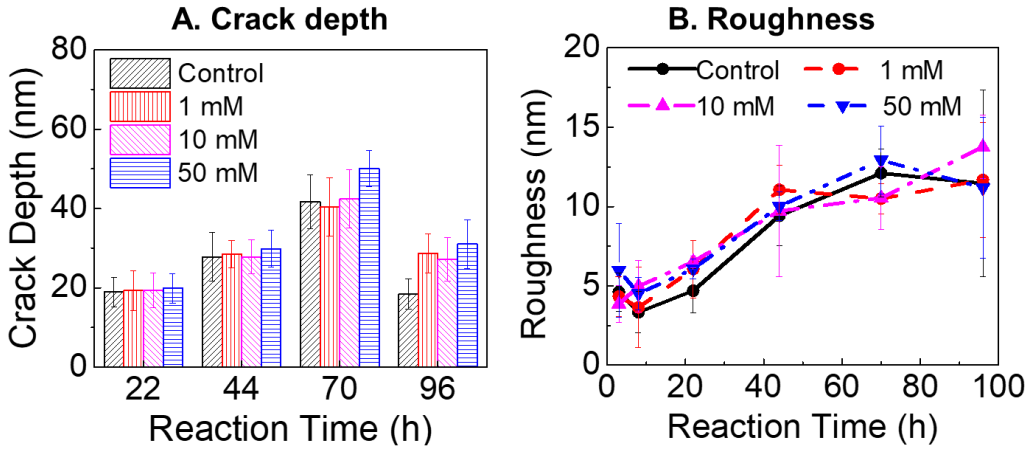

Figure 4 (**A**) Statistical crack depth and (**B**) roughness (R_q) of biotite basal surfaces after reaction with different concentrations of sulfate at 95 °C and 102 atm CO_2. For each sample, at least four locations on the sample surface were measured to determine the roughness. The depth of the cracks in sample surfaces were also measured from the AFM images by taking the average of 20 spots from four representative AFM images (Figure S2).

Figure 4A shows a statistical analyses of crack depths, made by taking the average of 80 spots where cracks were located in four representative AFM images. Consistent with ICP-OES results of indistinguishable biotite dissolution among the four reaction systems (Figure 1), the depths of the cracks formed were close after 22 and 44 h reactions. After a longer reaction time of 70 h with 50 mM sulfate, the cracks formed on biotite basal surfaces were slightly deeper, suggesting more biotite dissolution (Figure 1). We should note that detachments of surface cracked layers into the solutions after 96 h reactions made the crack depths observed smaller than those on 70 h samples. We also analyzed the changes in surface roughness, indicating overall surface morphology and texture, of reacted biotite samples over time (Figure 4B). Due to the formation of fibrous illite and cracks on biotite, the surface roughness increased over time. However, among the control and sulfate samples, the surface roughness of the reacted biotite samples was almost same, reflecting the similar surface morphologies of the samples reacted in the four systems.

Furthermore, the wettability alterations of reacted biotite basal surfaces were characterized and are shown in Figure 5. The contact angles for samples reacted in 1 mM sulfate systems were close to those of control samples (27°). While there were no significant differences in contact angles for samples reacted in 10 mM and 50 mM sulfate samples, they

were about 5° lower than for the control samples, indicating an enhanced biotite surface wettability. Based on our previous study,[53] chemical reactions altered biotite surface wettability, by changing the surface roughness, surface functional groups, and surface charge. In this study, we found that the alterations of biotite surface wettability by sulfate were mainly attributed to sulfate surface adsorption. As shown in the inset in Figure 2, the amount of adsorbed sulfate is much smaller in the 1 mM sulfate system than in the 10 mM and 50 mM sulfate systems. Therefore, biotite reacted with 1 mM sulfate did not show different surface wettability from the control samples. In the 10 mM and 50 mM sulfate systems, the higher amounts of sulfate adsorption could expose hydrophilic sulfate functional groups on biotite surfaces.[63-64] Moreover, the main aqueous sulfate species under the experimental pH was SO_4^{2-}. Adsorption of SO_4^{2-} onto edge sites exposed by cracks on biotite basal surfaces could also make more negatively charged surfaces. These two consequences of sulfate adsorption resulted in lower contact angles of the reacted biotite samples and enhanced their surface wettability. It has been reported that surface roughness contributed to more hydrophilic biotite surfaces.[53] Nonetheless, in this study, surface roughness was not the dominant mechanism for the sulfate effects on biotite wettability alterations. As shown in Figure 4B, after the same reaction times, the surface roughness values were close for biotite samples in all the four systems.

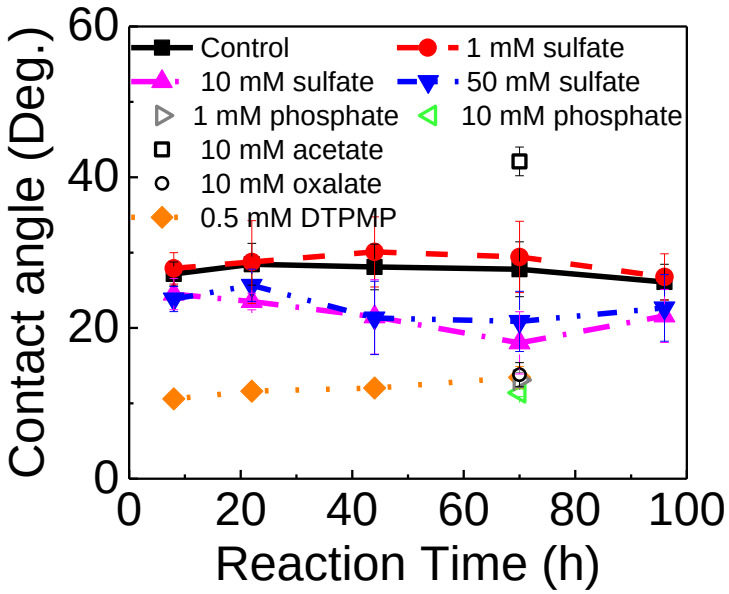

Figure 5 Contact angles of biotite basal surfaces after reactions in solutions of various aqueous chemistries over time at 95 °C and 102 atm of CO_2. The error bars are standard deviations of six measurements of duplicate samples in triplicate experiments. The data of phosphate and DTPMP are reproduced from refs. 52 (Copyright 2017 Royal Society of Chemistry), and refs 47, and 49 (Copyright 2018 American Chemical Society).

3.4 A Systematic Comparison of Sulfate Effects with Those of Other Inorganic/Organic Ligands

To better understand of the effects of complex brine compositions on surface chemistry changes, we compared sulfate (this study) with other inorganic/organic ligands (data obtained from our previous studies[47, 49-53]) (Figure 6). The relative M (M = K, Si, and Fe) indicates the ratios of M concentrations in the corresponding systems with various aqueous species to those in the control systems, and 70 h data is shown. Note that the aqueous ion concentrations are net concentrations (i.e., intrinsic biotite dissolution minus secondary

mineral precipitation). As shown in Figure 6, except for the 10 mM oxalate system, all other systems had interlayer K ratios close to 1, indicating no influence on K dissolution. These ratios of released K, mediated by ion exchange reactions, were the result of controlled ionic strengths and initial pH values.

The dissolution of framework cations is through proton-mediated or ligand-mediated reactions. For framework Si (Figure 6B), the ratios were greater than 1 with 50 mM sulfate, 10 mM phosphate, 10 mM oxalate, and 0.5 mM DTPMP (diethylenetriamine penta(methylene) phosphonate, a scale inhibitor), indicating their enhancement effects on biotite dissolution. Notably, oxalate significantly promoted biotite dissolution, suggested by the higher ratio of Si and Fe. The promoted mineral dissolution could create void spaces and increase reservoir porosity and affect the integrity of the shales. In the 10 mM oxalate system, the enhanced biotite dissolution released high concentrations of framework cations in solution, contributed to a final pH around 0.3 unit higher than for the control, and thus inhibited the release of interlayer K.[50] Regarding surface complexation, monodentate mononuclear complexes formed between sulfate/phosphate and biotite surface sites, while bidentate mononuclear complexes formed between oxalate and biotite. The latter complex type can strongly promote mineral dissolution. In addition to surface complexation, aqueous complexation, revealed by UV–Vis spectroscopy analyses, plays a role in the DTPMP system facilitating biotite dissolution.[47, 49]

For Fe (Figure 6C), ratios greater than 1 were observed with 50 mM sulfate and 10 mM oxalate. Although 10 mM phosphate and 0.5 mM DTPMP enhanced biotite dissolution, as suggested by Si, the ratios for Fe were smaller than 1. The differences in Fe ratios in these sulfate, oxalate, phosphate, and DTPMP systems resulted from their propensity to precipitate

with Fe. Fe-bearing phosphate/phosphonate minerals, such as $FePO_4 \cdot 2H_2O$, $AlPO_4$, $AlH_2PO_4(OH)_2$, and $Fe_{2.5}HNTMP$ (NTMP is a phosphonate), with solubility product constants (K_{sp}) lower than 10^{-19},[65-67] are significantly less soluble than Fe-sulfate/oxalate. In our previous work,[47, 52] After reaction with phosphate and DTPMP, we observed significant precipitation of strengite ($FePO_4 \cdot 2H_2O$) on biotite basal surfaces and amorphous Fe-bearing minerals in the solutions. The precipitation of these Fe-bearing minerals led to Fe ratios smaller than 1 in the phosphate and DTPMP systems. Furthermore, Al-bearing secondary precipitates were also observed in the phosphate and DTPMP systems. The significant formation of secondary minerals may alter pores and their connectivity in reservoir rocks, thus affecting their porosity and permeability. On the other hand, in the 10 mM acetate system, we observed Si and Fe ratios slightly lower than 1 (Figures 6B and 6C), which indicated that acetate slightly inhibited biotite dissolution through adsorption of acetic acid onto surface Si and Al sites influencing the protonation of biotite surfaces.

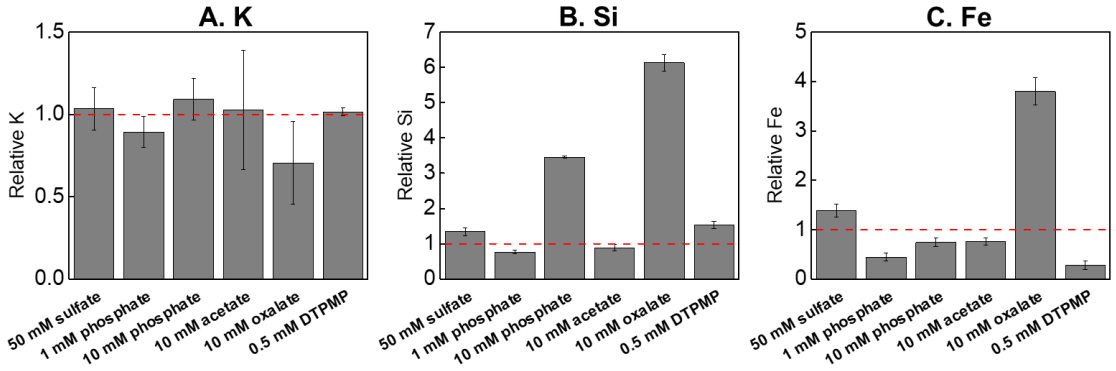

Figure 6 A comparison of sulfate effects with phosphate, acetate, oxalate, and DTPMP on cation concentrations during biotite dissolution at 95 °C and 102 atm CO_2. The relative K (**A**), Si (**B**), and Fe (**C**) value indicate the ratios of concentrations of cations in the corresponding systems to those in the control system after 70 h reactions. The data for sulfate

is from this work, for phosphate is from ref. 52 (Copyright 2017 Royal Society of Chemistry), for acetate and oxalate is from ref. 50 (Copyright 2015 American Chemical Society), and for phosphonate is from ref. 47 (Copyright 2018 American Chemical Society).

As a result of influenced biotite dissolution and secondary precipitation, different alterations of biotite surface morphology occurred. With 10 mM phosphate, 10 mM oxalate, and 0.5 mM DTPMP, formation of cracks was facilitated due to the enhanced biotite dissolution, observed within 8 h (Figure 3). The cracks on biotite surfaces made fibrous illite less observable (Figure 3C, E, F-8 h). Significant surface precipitation of Fe- and Al-bearing minerals was observed in the 10 mM phosphate and 0.5 mM DTPMP samples, resulting in rough surfaces (Figure 3C and 3F-70 h). Different from sulfate, phosphate, acetate, and oxalate, surface adsorption of large DTPMP molecules made the cracked biotite layers bend outwards (inset in Figure 3F-70 h).

We further compared the wettability alterations of biotite surfaces after reaction with different aqueous inorganic/organic species (Figure 4). Sulfate, phosphate, oxalate, and DTPMP enhanced biotite surface wettability, with lower contact angles observed. The adsorption of these chemical species, resulting in exposure of hydrophilic functional groups on biotite surfaces and more negative surface charged surfaces, is dominant over surface roughness in enhancing surface wettability. Also, with oxalate, XPS O 1s results showed that significant biotite dissolution induced a slightly higher density of hydroxyl groups (~91.2%) on reacted biotite surfaces (Table S2 and a detailed experimental description is available in S4) than on control samples (~89.2%). Although the changes in hydroxyl groups were not significant, the increase in hydroxyl groups might contribute to the enhanced biotite surface

wettability by oxalate. Differently, 10 mM acetate induced higher contact angles than the control sample, suggesting that biotite was altered to be more hydrophobic. Acetic acid was the dominant aqueous species in the 10 mM acetate system under the experimental conditions (pH = 3.2), and its adsorption would have the carboxylic groups pointed toward the mineral surface and leave a hydrophobic methyl group in the outer surface.

4. Conclusions

In this study, we report the effects of sulfate ions on biotite interfacial interactions under high temperature and high pressure conditions relevant to engineered subsurface operations. A sulfate concentration of 50 mM promoted biotite dissolution by 40%, mainly through monodentate mononuclear surface complexation. Sulfate adsorption enhanced biotite surface wettability. To systematically compare sulfate effects with those of other inorganic/organic ligands, Table 1 summarizes what we learned from all the experiments in the presence of complex ligands, which are abundant in brine. The ligands examined showed different effects on biotite dissolutions. Ligands that could form monodentate mononuclear (sulfate and phosphate) or bidentate mononuclear (oxalate) surface complexes promoted biotite dissolution, and the latter configuration of surface complexation induced greater dissolution. In addition, DTPMP, a ligand with more functional groups, promoted biotite dissolution through both aqueous complexation and surface complexation. Different from sulfate, acetate, and oxalate, the presence of phosphate and DTPMP, both having phosphate functional groups, significantly promoted precipitation of Fe- and Al-bearing secondary minerals. For all the inorganic and organic ligands, their surface adsorption dominantly

affected biotite surface wettability by changing surface functional groups and surface charges rather than surface roughness.

Table 1 A summary of field concentrations of abundant inorganic/organic ligands,[24-27, 36-37, 40-44] and their interactions with biotite, and consequent effects on dissolution, precipitation, and wettability.[47, 49-53]

	Sulfate	**Phosphate**	**Acetate**	**Oxalate**	**Phosphonate (DTPMP)**
Field concentration (mM)	10–50	0–0.02	16–250	0–5	~0.05
Interaction	surface complexation	monodentate mononuclear surface complexation	surface adsorption to Si & Al	bidentate mononuclear surface complexation	aqueous complexation & surface complexation
Dissolution	↑	↑↑	↓	↑↑↑	↑↑↑
Precipitation	--	↑↑↑	↑	↑↑	↑↑↑
Wettability	↑	↑↑↑	↓	↑↑↑	↑↑↑

Note: Different pH conditions may affect the interactions between inorganic/organic ligands with biotite. The information summarized here was obtained from experiments with pH values lower than 4.5. The number of arrows indicates the extent of the influence of the specific interactions. The direction of the arrows indicates promotion (upward) or inhibition (downward). The data for sulfate is from this current work, for phosphate is from ref. 52 (Copyright 2017 Royal Society of Chemistry), for acetate and oxalate (except for wettability, from the current work) is from ref. 50 (Copyright 2015 American Chemical Society), and for phosphonate is from refs. 47 and 49 (Copyright 2018 American Chemical Society).

Subsurface brine contains a wide spectrum of inorganic and organic ligands. The results summarized in this study suggest that, as a starting point, we can examine the

functional groups in the ligands and consider their general effects on mineral dissolution and secondary precipitation. The extents of these dissolution and precipitation reactions will further affect the porosity and permeability of subsurface reservoirs. By analyzing the possible functional groups exposed on mineral surfaces as a result of adsorption of aqueous chemical species, we can also obtain a first understanding of their effects on mineral wettability. However, we also note that coexisting ligands may compete with each other to suppress the effects of other ligands, or they may show synergetic effects of geochemical reactions of minerals.[29] Future studies investigating multi-ligand systems are needed.

Furthermore, the results presented in this study, using biotite as a model phyllosilicate, can provide useful insights into interfacial reactions of other abundant phyllosilicates at subsurface sites. Although some other phyllosilicates are less reactive than biotite, the time scale of geologic CO_2 storage is much longer than our experimental time. Those phyllosilicates may slowly react and ultimately result in similar alterations as biotite.

Electronic Supplementary Information

Details on the high temperature and high pressure experimental setup are in S1, thermodynamic calculations by GWB are in S2, AFM measurements are in S3, XPS measurements are in S4, and discussion on impact of CO_2 on the effect of sulfate is in S5.

Acknowledgments

This work was supported by the Center for Nanoscale Controls on Geologic CO_2, an Energy Frontier Research Center funded by the U.S. Department of Energy, Office of Science, Office of Basic Energy Sciences, via Grant DE-AC02-05CH11231. We also thank

the National Science Foundation's CAREER Award (EAR-1057117) and Washington University's Consortium for Clean Coal Utilization. The authors acknowledge Washington University's Nano Research Facility for use of ICP-OES. We also thank Professor James Ballard for carefully reviewing our manuscript.

References

1. *Subsurface Technology and Engineering Research, Development, and Demonstration (SubTER) Crosscut*; U.S. Department of Energy: 2017.
2. Orr, F. M., Onshore geologic storage of CO_2. *Science* **2009,** *325* (5948), 1656-1658.
3. Tokunaga, T. K., DLVO-based estimates of adsorbed water film thicknesses in geologic CO_2 reservoirs. *Langmuir* **2012,** *28* (21), 8001-8009.
4. Bondor, P., Applications of carbon dioxide in enhanced oil recovery. *Energ. Convers. Manage.* **1992,** *33* (5), 579-586.
5. Chiquet, P.; Broseta, D.; Thibeau, S., Wettability alteration of caprock minerals by carbon dioxide. *Geofluids* **2007,** *7* (2), 112-122.
6. Wang, S.; Edwards, I. M.; Clarens, A. F., Wettability phenomena at the CO_2–brine–mineral interface: implications for geologic carbon sequestration. *Environ. Sci. Technol.* **2012,** *47* (1), 234-241.
7. Shi, J.-Q.; Xue, Z.; Durucan, S., Supercritical CO_2 core flooding and imbibition in Tako sandstone—Influence of sub-core scale heterogeneity. *Int. J. Greenhouse Gas Control* **2011,** *5* (1), 75-87.
8. Shiraki, R.; Dunn, T. L., Experimental study on water–rock interactions during CO_2 flooding in the Tensleep Formation, Wyoming, USA. *Appl. Geochem.* **2000,** *15* (3), 265-279.
9. Saraji, S.; Goual, L.; Piri, M.; Plancher, H., Wettability of supercritical carbon dioxide/water/quartz systems: Simultaneous measurement of contact angle and interfacial tension at reservoir conditions. *Langmuir* **2013,** *29* (23), 6856-6866.
10. Espinoza, D. N.; Santamarina, J. C., Water–CO_2–mineral systems: Interfacial tension, contact angle, and diffusion—Implications to CO_2 geological storage. *Water Resour. Res.* **2010,** *46* (7), W07537.
11. Busch, A.; Alles, S.; Gensterblum, Y.; Prinz, D.; Dewhurst, D. N.; Raven, M. D.; Stanjek, H.; Krooss, B. M., Carbon dioxide storage potential of shales. *Int. J. Greenhouse Gas Control* **2008,** *2* (3), 297-308.
12. Metz, B.; Davidson, O.; De Coninck, H.; Loos, M.; Meyer, L. *IPCC special report on carbon dioxide capture and storage: Prepared by Working Group III of the Intergovernmental Panel on Climate Change*; IPCC: Cambridge University Press: Cambridge, United Kingdom and New York, USA, **2005**.
13. Montgomery, C. T.; Smith, M. B., Hydraulic fracturing: history of an enduring technology. *Journal of Petroleum Technology* **2010,** *62* (12), 26-40.
14. Rahm, D., Regulating hydraulic fracturing in shale gas plays: The case of Texas. *Energy Policy* **2011,** *39* (5), 2974-2981.
15. Bourg, I. C., Sealing Shales versus Brittle Shales: A Sharp Threshold in the Material Properties and Energy Technology Uses of Fine-Grained Sedimentary Rocks. *Environ. Sci. Technol. Lett.* **2015,** *2* (10), 255-259.
16. Credoz, A.; Bildstein, O.; Jullien, M.; Raynal, J.; Pétronin, J.-C.; Lillo, M.; Pozo, C.; Geniaut, G., Experimental and modeling study of geochemical reactivity between clayey caprocks and CO_2 in geological storage conditions. *Energy Procedia* **2009,** *1* (1), 3445-3452.

17. Kaszuba, J. P.; Janecky, D. R.; Snow, M. G., Carbon dioxide reaction processes in a model brine aquifer at 200 C and 200 bars: implications for geologic sequestration of carbon. *Appl. Geochem.* **2003,** *18* (7), 1065-1080.
18. Kaszuba, J. P.; Janecky, D. R.; Snow, M. G., Experimental evaluation of mixed fluid reactions between supercritical carbon dioxide and NaCl brine: Relevance to the integrity of a geologic carbon repository. *Chem. Geol.* **2005,** *217* (3), 277-293.
19. Blatt, H.; Tracy, R.; Owens, B., *Petrology: igneous, sedimentary, and metamorphic*. Macmillan: 2006.
20. Brown, G., Crystal structures of clay minerals and related phyllosilicates. *Phil. Trans. R. Soc. Lond. A* **1984,** *311* (1517), 221-240.
21. Moore, D. M.; Reynolds, R. C., *X-ray Diffraction and the Identification and Analysis of Clay Minerals*. Oxford university press New York: 1989; Vol. 332.
22. Sparks, D. L., *Environmental soil chemistry*. Elsevier Science: London, UK, 2003.
23. Brantley, S. L., Kinetics of mineral dissolution. In *Kinetics of water-rock interaction*, Springer: 2008; pp 151-210.
24. Keller, S. J., *Analyses of subsurface brines of Indiana*. State of Indiana, Department of Natural Resources, Geological Survey: 1983.
25. Kharaka, Y.; Hanor, J., Deep fluids in the continents: I. Sedimentary basins. *Treatise Geochem* **2003,** *5*, 499-540.
26. Soong, Y.; Goodman, A.; McCarthy-Jones, J.; Baltrus, J., Experimental and simulation studies on mineral trapping of CO_2 with brine. *Energ. Convers. Manage.* **2004,** *45* (11-12), 1845-1859.
27. Wandrey, M.; Pellizari, L.; Zettlitzer, M.; Würdemann, H., Microbial community and inorganic fluid analysis during CO_2 storage within the frame of CO2SINK–Long-term experiments under in situ conditions. *Energy Procedia* **2011,** *4*, 3651-3657.
28. Xu, T.; Apps, J. A.; Pruess, K.; Yamamoto, H., Numerical modeling of injection and mineral trapping of CO_2 with H_2S and SO_2 in a sandstone formation. *Chem. Geol.* **2007,** *242* (3), 319-346.
29. Min, Y.; Kubicki, J. D.; Jun, Y.-S., Plagioclase Dissolution during CO_2–SO_2 Cosequestration: Effects of Sulfate. *Environ. Sci. Technol.* **2015,** *49* (3), 1946-1954.
30. Li, Q.; Lim, Y. M.; Jun, Y.-S., Effects of Sulfate during CO_2 Attack on Portland Cement and Their Impacts on Mechanical Properties under Geologic CO_2 Sequestration Conditions. *Environ. Sci. Technol.* **2015,** *49* (11), 7032-7041.
31. Karimi, M.; Al-Maamari, R. S.; Ayatollahi, S.; Mehranbod, N., Wettability alteration and oil recovery by spontaneous imbibition of low salinity brine into carbonates: Impact of Mg^{2+}, SO_4^{2-} and cationic surfactant. *Journal of Petroleum Science and Engineering* **2016,** *147*, 560-569.
32. Karoussi, O.; Hamouda, A. A., Imbibition of sulfate and magnesium ions into carbonate rocks at elevated temperatures and their influence on wettability alteration and oil recovery. *Energy Fuels* **2007,** *21* (4), 2138-2146.
33. Zhang, P.; Austad, T., Wettability and oil recovery from carbonates: Effects of temperature and potential determining ions. *Colloids Surf., A.* **2006,** *279* (1), 179-187.
34. Tabrizy, V. A.; Hamouda, A.; Denoyel, R., Influence of magnesium and sulfate ions on wettability alteration of calcite, quartz, and kaolinite: surface energy analysis. *Energy Fuels* **2011,** *25* (4), 1667-1680.

35. Karimi, M.; Al-Maamari, R. S.; Ayatollahi, S.; Mehranbod, N., Impact of Sulfate Ions on Wettability Alteration of Oil-Wet Calcite in the Absence and Presence of Cationic Surfactant. *Energy Fuels* **2016,** *30* (2), 819-829.
36. Keller, S. J. *Analyses of subsurface brines of Indiana*; State of Indiana, Department of Natural Resources, Geological Survey: Bloomington, 1983.
37. Kharaka, Y. K.; Thordsen, J. J.; Hovorka, S. D.; Seay Nance, H.; Cole, D. R.; Phelps, T. J.; Knauss, K. G., Potential environmental issues of CO_2 storage in deep saline aquifers: Geochemical results from the Frio-I Brine Pilot test, Texas, USA. *Appl. Geochem.* **2009,** *24* (6), 1106-1112.
38. Stringfellow, W. T.; Domen, J. K.; Camarillo, M. K.; Sandelin, W. L.; Borglin, S., Physical, chemical, and biological characteristics of compounds used in hydraulic fracturing. *J. Hazard. Mater.* **2014,** *275*, 37-54.
39. Amjad, Z., *Mineral scale formation and inhibition*. Springer Science & Business Media: 2013.
40. Tomson, M.; Fu, G.; Watson, M.; Kan, A., Mechanisms of mineral scale inhibition. *Soc. Petrol. Eng. J.* **2002,** *18* (3), 192-199.
41. García, A. V.; Thomsen, K.; Stenby, E. H., Prediction of mineral scale formation in geothermal and oilfield operations using the Extended UNIQUAC model: part II. Carbonate-scaling minerals. *Geothermics* **2006,** *35* (3), 239-284.
42. Kan, A. T.; Fu, G.; Tomson, M. B.; Al-Thubaiti, M.; Xiao, A. J., Factors affecting scale inhibitor retention in carbonate-rich formation during squeeze treatment. *Soc. Petrol. Eng. J.* **2004,** *9* (03), 280-289.
43. Oddo, J.; Tomson, M., Why scale forms in the oil field and methods to predict it. *SPE Prod. Facil.* **1994,** *9* (01), 47-54.
44. Tollefson, J., Secrets of fracking fluids pave way for cleaner recipe. *Nature* **2013,** *501* (7466), 146.
45. Kononova, S.; Nesmeyanova, M., Phosphonates and their degradation by microorganisms. *Biochemistry (Moscow)* **2002,** *67* (2), 184-195.
46. Demadis, K. D.; Ketsetzi, A., Degradation of Phosphonate-Based Scale Inhibitor Additives in the Presence of Oxidizing Biocides:"Collateral Damages" in Industrial Water Systems. *Sep. Sci. Technol.* **2007,** *42* (7), 1639-1649.
47. Zhang, L.; Kim, D.; Jun, Y.-S., The Effects of Phosphonate-Based Scale Inhibitor on Brine−Biotite Interactions under Subsurface Conditions. *Environ. Sci. Technol.* **2018,** *52* (10), 6042-6049.
48. Zhang, L.; Jun, Y.-S., The Role of Fe-Bearing Phyllosilicates in DTPMP Degradation under High-Temperature and High-Pressure Conditions. *Environ. Sci. Technol.* **2018,** *52* (16), 9522-9530.
49. Zhang, L.; Kim, D.; Jun, Y.-S., Effects of Phosphonate Structures on Brine–Biotite Interactions under Subsurface Relevant Conditions. *ACS Earth Space Chem* **2018,** *2* (9), 946-954.
50. Zhang, L.; Jun, Y.-S., Distinctive Reactivities at Biotite Edge and Basal Planes in the Presence of Organic Ligands: Implications for Organic-Rich Geologic CO_2 Sequestration. *Environ. Sci. Technol.* **2015,** *49* (16), 10217-10225.

51. Jun, Y.-S.; Zhang, L.; Min, Y.; Li, Q., Nanoscale Chemical Processes Affecting Storage Capacities and Seals during Geologic CO_2 Sequestration. *Acc. Chem. Res.* **2017,** *50* (7), 1521-1529.
52. Zhang, L.; Kim, D.; Kim, Y.; Wan, J.; Jun, Y.-S., Effects of Phosphate on Biotite Dissolution and Secondary Precipitation under Conditions Relevant to Engineered Subsurface Processes. *Phys. Chem. Chem. Phys.* **2017,** *19*, 29895-29904.
53. Zhang, L.; Kim, Y.; Jung, H.; Wan, J.; Jun, Y.-S., Effects of Salinity-Induced Chemical Reactions on Biotite Wettability Changes under Geologic CO_2 Sequestration Conditions. *Environ. Sci. Technol. Lett.* **2016,** *3* (3), 92-97.
54. Bradshaw, J.; Cook, P., Geological sequestration of carbon dioxide. *Environ. Geosci.* **2001,** *8* (3), 149-151.
55. Xu, T.; Kharaka, Y. K.; Doughty, C.; Freifeld, B. M.; Daley, T. M., Reactive transport modeling to study changes in water chemistry induced by CO_2 injection at the Frio-I Brine Pilot. *Chem. Geol.* **2010,** *271* (3), 153-164.
56. Shao, H. B.; Ray, J. R.; Jun, Y. S., Dissolution and Precipitation of Clay Minerals under Geologic CO_2 Sequestration Conditions: CO_2-Brine-Phlogopite Interactions. *Environ. Sci. Technol.* **2010,** *44* (15), 5999-6005.
57. Martell, A. E.; Smith, R. M., *Critical stability constants*. Springer: 1974; Vol. 1.
58. Serna, C. J.; White, J.; Hem, S. L., Anion-Aluminum Hydroxide Gel Interactions 1. *Soil Sci. Soc. Am. J.* **1977,** *41* (5), 1009-1013.
59. Furrer, G.; Stumm, W., The coordination chemistry of weathering: I. Dissolution kinetics of δ-Al_2O_3 and BeO. *Geochim. Cosmochim. Acta* **1986,** *50* (9), 1847-1860.
60. Loewenstein, W., The distribution of aluminum in the tetrahedra of silicates and aluminates. *Am. Mineral.* **1954,** *39*, 92-96.
61. Shao, H.; Ray, J. R.; Jun, Y.-S., Effects of organic ligands on supercritical CO_2-induced phlogopite dissolution and secondary mineral formation. *Chem. Geol.* **2011,** *290* (3-4), 121-132.
62. Hu, Y.; Ray, J. R.; Jun, Y. S., Biotite-brine interactions under acidic hydrothermal conditions: fibrous illite, goethite, and kaolinite formation and biotite surface cracking. *Environ. Sci. Technol.* **2011,** *45* (14), 6175-6180.
63. Plumridge, T. H.; Steel, G.; Waigh, R. D., Geometry-based simulation of the hydration of small molecules. *PhysChemComm* **2000,** *3* (8), 36-41.
64. Bergstroem, P. A.; Lindgren, J.; Kristiansson, O., An IR study of the hydration of perchlorate, nitrate, iodide, bromide, chloride and sulfate anions in aqueous solution. *J. Phys. Chem.* **1991,** *95* (22), 8575-8580.
65. Friedfeld, S. J.; He, S.; Tomson, M. B., The temperature and ionic strength dependence of the solubility product constant of ferrous phosphonate. *Langmuir* **1998,** *14* (13), 3698-3703.
66. Iuliano, M.; Ciavatta, L.; De Tommaso, G., On the solubility constant of strengite. *Soil Sci. Soc. Am. J.* **2007,** *71* (4), 1137-1140.
67. Ferguson, J. F.; King, T., A model for aluminum phosphate precipitation. *J. Water Pollut. Control Fed.* **1977**, 646-658.

Table of Contents

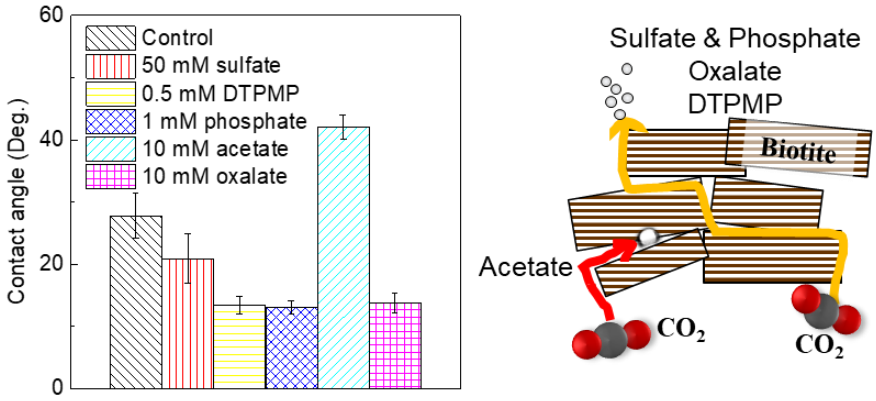

Anions affect water-biotite interfacial interactions to different extents and subsequently alter surface wettability.